Biosensors and Bioelectronics 126 (2019) 647–656

Contents lists available at ScienceDirect

Biosensors and Bioelectronics

journal homepage: www.elsevier.com/locate/bios

Graphene-oxide quenching-based molecular beacon imaging of exosome-mediated transfer of neurogenic miR-193a on microfluidic platform

Hyun Jeong Oh[a,b,d], Jaehoon Kim[d], Hyejin Park[d], Seok Chung[d,*], Do Won Hwang[a,b,c,**], Dong Soo Lee[a,b,***]

[a] Department of Nuclear Medicine, Seoul National University College of Medicine, 101 Daehak-ro, Jongno-gu, Seoul 110-744, Republic of Korea
[b] Department of Molecular Medicine and Biopharmaceutical Sciences, Graduate School of Convergence Science and Technology, Seoul National University, 101 Daehak-ro, Jongno-gu, Seoul 110-744, Republic of Korea
[c] Medical Research Center, Institute of Radiation Medicine, Seoul National University College of Medicine, 101 Daehak-ro, Jongno-gu, Seoul 110-744, Republic of Korea
[d] School of Mechanical Engineering, Korea University, 145 Anam Dong, Seongbuk, Seoul 02841, Republic of Korea

ARTICLE INFO

Keywords:
Molecular beacon sensor
miRNA-193a
Peptide nucleic acid (PNA)
Graphene oxide (GO)
Exosome-mediated neurogenesis
Microfluidic platform

ABSTRACT

Graphene-oxide (GO) quenching-based molecular beacon was developed for rapid and sensitive detection of RNAs in living cells and tissues. Here, we applied GO quenching-based molecular beacon sensor to visualize neurogenic miR-193a levels delivered *via* exosomes during cell-non-autonomous neurogenesis in neural progenitor cells on a microfluidic platform. Exosomal transport was visualized using CD63-RFP plasmid vector, and FAM-labeled peptide nucleic acid (PNA) probe for the miR-193 sequence was designed to detect endogenous miR-193 expression. Fluorescence signals of FAM-PNA193a-GO were recovered in dibutyryl-cAMP-induced F11 cells, resulting from increased expression of miR-193a after neuronal differentiation. We observed delivery of miR-193a-containing exosomes released from differentiated donor F11 cells to recipient undifferentiated F11 cells. Fluorescence recovery was evident in exosome-stimulated recipient individual F11 cells in the microfluidic system. We propose molecular beacon imaging using PNA-GO complex for visualization of individual cellular expression of mature microRNAs. This system reveals the precise spatial localization and temporal sequences of mature miRNAs by intercellular exosomal delivery of messages for processes such as cell-non-autonomous neurogenesis.

1. Introduction

Neurogenesis is associated with dynamic changes of microRNA (miRNA) expression. miRNAs are proposed to be responsible for determining cellular status of differentiating neural stem cells or progenitor cells (Sayed and Abdellatif, 2011; Sun et al., 2010). miRNAs degrade target mRNAs, inhibit translation of mRNAs in a sequence-specific manner (Bartel, 2004; He and Hannon, 2004; Kosaka et al., 2010; Novina and Sharp, 2004), and play roles in cell proliferation (Delaloy et al., 2010; Niu et al., 2013) and differentiation (Åkerblom and Jakobsson, 2014; Chen et al., 2004; Makeyev et al., 2007). Several miRNAs such as let-7, miR-124, miR-9, and miR-193a are known to be involved in neuronal differentiation of neural stem cells or progenitor cells (Eskildsen et al., 2011; Gagan et al., 2011; Jing et al., 2011; Karbiener et al., 2011; Oh et al., 2017).

Neurogenic miRNA was reported to regulate neurogenesis *via* delivery within exosomes from donor to recipient cells (Delaloy et al., 2010; Zernecke et al., 2009). Exosomes contain many peptides, nucleic acids, and miRNAs involved in the regulation of proliferation and differentiation (Åkerblom and Jakobsson, 2014; Chen et al., 2004; Delaloy et al., 2010; Deregibus et al., 2007; Makeyev et al., 2007; Niu et al., 2013; Pegtel et al., 2010; Ratajczak et al., 2006; Skog et al., 2008; Zernecke et al., 2009). We observed that exosomes from differentiated neural progenitor cells delivered neurogenic miR-193a contained within them to promote neurogenesis of neighboring undifferentiated clones. Functional consequences of miR-193a were verified with bioluminescence imaging using luciferase with a sense sequence in the 3′ untranslated region (UTR) against the antisense sequence of miR-193a (Kim et al., 2008; Ko et al., 2009; Tani et al., 2010) using the prototypical method for analysis of mature miRNA action (Hwang and Lee,

* Corresponding author.
** Corresponding author at: Medical Research Center, Institute of Radiation Medicine, Seoul National University College of Medicine, Seoul, Republic of Korea.
*** Correspondence to: Department of Nuclear Medicine, Seoul National University Hospital, 101 Daehak-ro, Jongno-gu, Seoul 110-744, Republic of Korea.
E-mail addresses: sidchung@korea.ac.kr (S. Chung), hdw6592@snu.ac.kr (D.W. Hwang), dsl@plaza.snu.ac.kr (D.S. Lee).

https://doi.org/10.1016/j.bios.2018.11.027
Received 5 September 2018; Received in revised form 8 November 2018; Accepted 18 November 2018
Available online 20 November 2018
0956-5663/

2012; Ko et al., 2009; Lee et al., 2008; Oh et al., 2013).

Luciferase reporter imaging provides excellent results without background *in vivo* and *in vitro*; however, luciferase activity is decreased by target miRNA, which is termed a "signal-off system." Mature miRNA activity is observed by examining the degree of decreased reporter activity. An issue with the signal-off system is that the decreased in reporter signal can also be due to cell conditions such as cell viability. The molecular beacon was proposed as a "signal-on system" for monitoring RNA expression (Peng et al., 2005; Tan et al., 2004). We reported the use of fluorescence nanoparticle-based molecular beacon system for monitoring miRNA expression (Hwang et al., 2010). Graphene-oxide quenching-based detection system adopts the same signal-on strategy to successfully detect the presence of multiplex miRNAs in live cultured cells (Ryoo et al., 2013).

Neuronal miRNAs turn over rapidly in retinal, hippocampal and cortical neurons depending upon stimuli or activity (Krol et al., 2010) and are transported to dendrites as pre-miRNA to be converted to mature miRNA in response to activity-dependent stimuli (Calin and Croce, 2006; Kosaka et al., 2010; Pritchard et al., 2012). Development of a sensing platform for detection of the expression levels of specific mature miRNAs will enable elucidation, of the spatial localization and transient actions of miRNAs in neuronal cell bodies and dendrites.

Therefore, an effective sensing method for miRNAs will be crucial for detection of various cellular events (Li et al., 2009; Wang et al., 2011). Recently, various sensing methods have been developed based on label-free probe for direct miRNA detection including molecular beacon (Hartig et al., 2004), surface plasmon resonance (SPR) (Fang et al., 2006) and surface-enhanced Raman spectroscopy (SERS) (Driskell and Tripp, 2010). Among these, the fluorescence-based molecular beacon system has been extensively employed for miRNA detection, due to its high sensitivity and selectivity, as well as its simple, robust, and accurate high-throughput miRNA profiling in living cells (Duan et al., 2011; Pu et al., 2010; Ran et al., 2015; Shi et al., 2016).

Graphene oxide and its π-π stacking interaction for absorption and release of fluorescent dye-labeled peptide nucleic acid (PNA) probes by hydrogen bonds of endogenous miRNA were used for multiplexed miRNA detection (Ryoo et al., 2013) and for differential detection of miRNAs showing single-base pair mismatches (Lee et al., 2015). Graphene's fluorescence quenching capability is manifested when it attaches to fluorescent dye-labeled PNA and fluorescence is recovered upon detachment of PNA from graphene due to the complimentary sequences of endogenous miRNA to those of PNA probes. PNA, a non-natural nucleic acid analog, has the backbones held by uncharged amide bonds which differs from the negatively charged-phosphodiester bonds of classical nucleic acids (Hanvey et al., 1992; Lu et al., 2012).

The miRNA sensing strategy is based on the recovery of fluorescence of the quenched dye-labeled PNA as a probe that was tightly bound to the surface of GO as a fluorescence quencher and subsequent recovery of the fluorescence upon addition of target miRNA (Fig. 1). This miRNA sensing platform allows high sensitivity and specificity toward target miRNA with low background signal. Microfluidic cell culture assay can be used for observation and capturing of various phenomena between cells (Wang et al., 2018; Lee et al., 2017) and to simulate *in vivo* cellular interactions under *in vitro* setting using tissue-mimetic architectures with hydrogel-incorporating microfluidic device and interstitial mimicking fluid (Shin et al., 2012).

Here, we applied the above miRNA sensing probes using dye-labeled PNA and GO for sensitive and real-time monitoring of specific miRNAs in living cells on microfluidic devices. We examined individual recipient neural progenitor cells receiving exosomes containing relevant miRNAs and responding to the cell-exosome fusion by commencing differentiation into the neurons (Oh et al., 2017). In our previous study (Oh et al., 2017), we established that the microfluidic platform could visualize convective exosomal transport and exosome-mediated communication between undifferentiated and differentiated cells. Based on this study (Oh et al., 2017), in this investigation, we established molecular beacon imaging to detect endogenous miRNA expression based on fluorescence dye-labeled PNA-GO beacon during exosome-mediated neurogenesis in the hydrogel-incorporating microfluidic platform.

2. Experimental section

2.1. Cell culture

F11 cells, rat dorsal root ganglion, mouse neuroblastoma hybrid cells, and mouse neural stem cells (NE-4C) were cultured in Dulbecco's modified Eagle's medium (DMEM, Gibco) supplemented with 10% fetal bovine serum (FBS; Gibco), 10 U/mL penicillin, and 10 μg/mL streptomycin in a humidified atmosphere of 5% CO_2 at 37 °C. To induce neuronal differentiation, F11 cells were incubated with DMEM containing 0.5% FBS and 1 mM dibutyryl cyclic AMP (db-cAMP, Sigma-Aldrich) or transfected (Lipofectamine2000; Invitrogen) with miR-193a (Ambion®) for 3 days.

2.2. Synthesis of PNA and DNA oligomers

The fluorescent dye (FAM)-labeled PNA probe was synthesized by Panagene Inc (HPLC profiles and MS spectra of all FAM-labeled PNA probes are represented in Supplementary information Fig. S1). The sequences of oligomers were 5′-ACTGGGACTTTGTAGGCCAGTT-3′ (FAM-PNA193a complementary oligomer) and 5′- TTGACCGGATGTT TCAGGGTCA-3′ (FAM-PNAscr complementary oligomer). All PNA probes were 22-mer in length (Supplementary information Table S1).

2.3. Quantitative RT-PCR analysis

Total RNA from differentiated F11 cells was prepared using Trizol (Invitrogen) and mirVana™ miRNA Isolation Kit (Ambion®). Isolated RNA was analyzed for purity and concentration in a Nanodrop-1000 Spectrophotometer (Thermo Scientific). The cDNA samples for miRNA was prepared by reverse transcription (RT) with the miRNA 1st-strand cDNA synthesis kit (Agilent Technologies). RT-PCR amplification was performed using ABI® 7500 (Applied Biosystems™) with the TaKaRa SYBR Green Master mix (Clontech Laboratories), which is specific for mature miRNA sequences. PCR primer for miR-193a was 5′-AACTGG CCTACAAAGTCCCAGT-3′ (forward) and the universal reverse primer was used for reverse primer. Relative values were normalized to U6 snRNA as an internal control. All experiments were performed in triplicate.

2.4. miR-193a detection using GO-PNA complexes

FAM-PNA probe (40 pmol per probe) was mixed with a series of GO (Lemonex Inc) solution, concentrations ranging from 0.1 μg to 0.9 μg in 100 μL of buffer (Tris-HCl, pH 7.5) for 15 min at room temperature (FT-IR spectrum of GO is shown in Supplementary information Fig. S1). The quenched fluorescence signals were monitored after the formation of FAM-PNA probe-GO complex. FAM-PNA-GO complex solution was mixed with various concentrations (2.5–40 pmol in 50 μL of buffer [Tris-HCl, pH 7.5]) of target oligomers with the complementary sequence. Fluorescence signals were measured using a Varioskan Flash Multimode Reader (Thermo Fisher Scientific). The fluorescence images of mixtures in a 96-well black plate were obtained using IVIS-100 imaging system (Xenogen).

2.5. miR-193a detection in differentiated cells

F11 cells were seeded on 6-well plates at 1.5×10^5 cells per well and incubated with DMEM containing 0.5% FBS and 1 mM db-cAMP (Sigma-Aldrich) for 3 days. FAM-PNA probe (100 pmol per probe) was mixed with GO (1 μg) in opti-MEM media (Invitrogen) for 15 min at

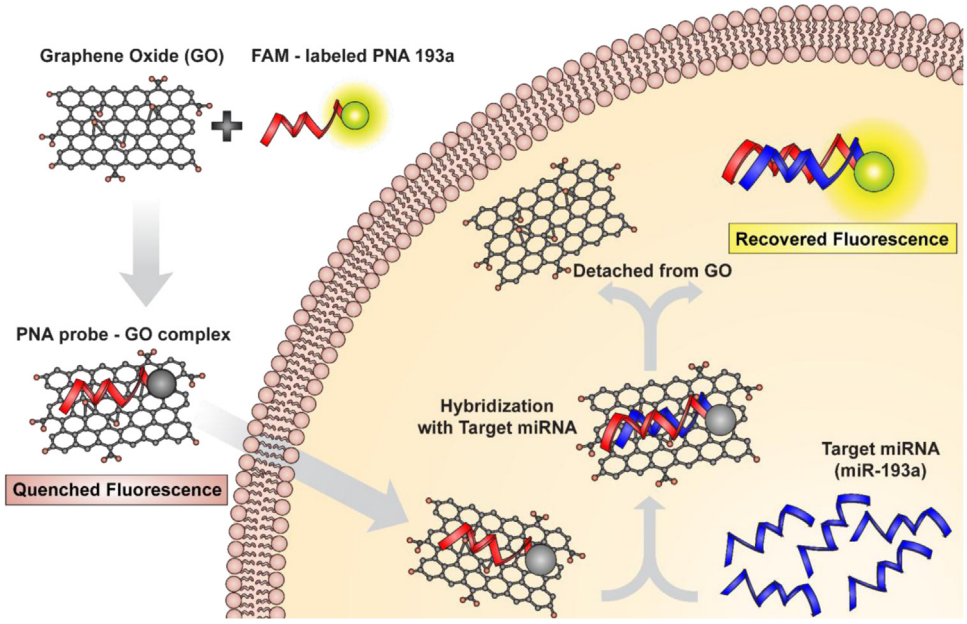

Fig. 1. Scheme of strategy for miR-193a sensing based on graphene oxide (GO) and peptide nucleic acid (PNA) in differentiated neural cells.

room temperature. The FAM-PNA193a-GO complexes were treated to F11 cells for 14 h at 37 °C and then vigorously washed three times with phosphate-buffered saline (PBS). The cells were fixed with 4% paraformaldehyde (PFA). Nuclei were counterstained with 4′-6-diamidino-2-phenylindole (DAPI, Vector Laboratories). Fluorescent images were obtained using a FV1000 confocal laser scanning microscope (Olympus).

2.6. Cytotoxicity assay of GO

F11 and NE-4C cells were seeded at 1×10^4 cells per well in a 24-well cell culture plate and maintained for 24 h. The cells were incubated with GO (at concentrations ranging from 0 to 50 μg/mL) in opti-MEM and incubated for 14 h at 37 °C. Following GO treatment, cells were rinsed with opti-MEM, and 20 μL of Cell Counting Kit-8 (CCK-8) solution (Dojindo, Rockville, MD) was added to each well containing 100 μL of opti-MEM. The cells were incubated for 2–3 h until color developed. Subsequently, 100 μL of the solution was transferred to a 96-well plate. The absorbance was measured at 450 nm using a GloMax®-Discover Microplate Reader (Promega, Fitchburg, WI).

2.7. Microfluidic device fabrication

The microfluidic co-culture system was composed of polydimethylsiloxane (PDMS; Sylgard 184; Dow Corning). The SU-8 photoresist pattern master (MicroChem) was used as a master mold, using a conventional soft lithography process to replicate the microchannel-patterned PDMS. PDMS was mixed with the curing agent at a 10:1 wt ratio, poured onto the wafer, and cured by baking in an oven at 60 °C for 8 h. The PDMS replica was detached from the wafer, and all reservoir patterns of the PDMS replica were punched by dermal biopsy punches (a 6 mm punch for media reservoirs and a 1 mm punch for gel filling reservoirs). The PDMS replica and glass coverslip were sterilized and bonded together *via* oxygen plasma (Femto Science) and placed at 60 °C in an oven for at least 48 h to restore hydrophobicity of the microchannel surfaces.

2.8. Co-culture of F11 cells in the microfluidic system

Type 1 collagen ECM (2 mg/mL; BD Biosciences) was diluted to 2 mg/mL in a mixture of 10× PBS (Gibco) and distilled deionized water. The pH of the hydrogel solution was adjusted to 7.4 with 0.5 N NaOH. Type 1 collagen ECM was inoculated into hydrogel channels and gelled for 30 min. The cell culture channel was then filled with medium to prepare cell seeding. F11 cells (donor cells) were seeded into the cell culture channel (left channel), and conditioned medium was added into the right cell culture channel. After cell attachment, the medium in the left channel which contained donor cells of the differentiated group, was replaced with differentiation medium (DMEM containing 0.5% FBS and 1 mM db-cAMP) for 48 h. DiI-labeled F11 cells (recipient cells) were seeded into the cell culture channel (right) and co-cultured with donor cells at 37 °C in 5% CO_2 for 3 days. Density of F11 cells (donor and recipient) suspended in conditioned medium was 1×10^6 cells/mL. Three days after co-culture, FAM-PNA probes (100 pmol per probe) mixed with GO (1 μg) in opti-MEM media (Invitrogen) were incubated for 15 min at room temperature. The FAM-PNA193a-GO complexes were treated with recipient F11 cells (right cell culture channel) for 14 h at 37 °C and then vigorously washed three times with PBS. The cells were fixed with 4% PFA. Nuclei were counterstained with 4′-6-diamidino-2-phenylindole (DAPI, Vector Laboratories). Fluorescent images were obtained using a FV1000 confocal laser scanning microscope (Olympus).

2.9. Two-step simulation of donor-released exosome transport

The concentration profiles of exosomes by convection (laminar flow) and diffusion were simulated using COMSOL Multiphysics (COMSOL, Stockholm, Sweden) software. The convective transport was designed by hydrostatic pressure differences in the case of daily medium addition to all reservoirs. The diffusion coefficients for exosomes in culture medium and type 1 collagen gel were calculated from the size (50–200 nm) using Einstein relation and the stochastic model (Pluen et al., 1999) (Supplementary information Table S2). Diffusive transport was simulated using a time transient model (0–24 h, Supplementary information Fig. S2).

2.10. Simulation of exosome concentration released from nD-F11 cells

The diffusive transport of exosomes released from nD-F11 cells to recipient cells was simulated using a time transient model for 24 h. The exosomes released from F11 cells were quantified using CD63-RFP fluorescence images (Supplementary information Fig. S3A). Exosome

production rate was calculated as a molecular concentration (3.878×10^{-14}). The nD-F11 cell population was assumed to be 15% of all recipient cells quantified from fluorescence images (Supplementary information Fig. S3B).

2.11. Statistical analysis

Results of all experiments were collected from three or four independent experiments for each sample. Data are presented as means ± standard deviation (SD). The Student's *t*-test was used to calculate *P* values. *P*-values < 0.005 were considered statistically significant.

3. Results

3.1. Neurogenesis of neural progenitor F11 cells by miR-193a

In our earlier work, we identified that miR-193a was involved in Ngn1-induced neurogenesis. We validated that miR-193a was highly expressed in differentiated neural cells by Ngn1 or db-cAMP and confirmed the neurogenic function of miR-193a in neural progenitor cells. To measure miR-193a expression in differentiating neural cells, F11 cells were treated with differentiation media containing db-cAMP for 3 days. Unlike undifferentiated F11 cells (UD-F11 cells), differentiated F11 cells (D-F11 cells) showed a neurite outgrowth and the expression of the neural marker, Tuj-1 (Fig. 2A). In qRT-PCR, the expression of miR-193a was quantified; a high amount of miR-193a was only detected in D-F11 cells (Fig. 2B). To validate the effects of miR-193a on neurogenesis, F11 cells were transfected with miR-scr or miR-193a for 3 days to induce neurogenesis. Normal F11 cell morphology was maintained, and most of the F11 cells underwent proliferation when treated with miR-scr. However, F11 cells transfected with miR-193a showed a neurite outgrowth pattern at 3 days after transfection. Tuj-1 expression was examined by immunofluorescence staining (Supplementary information Fig. S4A) and qRT-PCR analysis (Supplementary information Fig. S4B). Tuj-1 was more highly expressed in F11 cells transfected with miR-193a, compared to F11 cells treated with miR-scr (Supplementary information Fig. S4A and B). In summary, miR-193a was induced during neurogenesis in F11 cells and could induce neurogenesis when transfected.

3.2. FAM-PNA-GO complexes as sequence-specific molecular beacon

We tested the fluorescence quenching of FAM-PNAscr or FAM-PNA193a (fluorescent dye-conjugated PNA probe) based on GO attachment. Fluorescence of FAM-PNAscr or FAM-PNA193a solution (40 pmol) was completely quenched at 0.4 μg of GO (Fig. 3A). We used FAM-PNAscr-GO or FAM-PNA193a-GO mixture at a ratio 40 pmol: 0.4 μg for subsequent experiments. PNA193a probe had the complementary sequence to miR-193a. FAM-PNA-GO complex recovered the fluorescence of miR-193a but not that of miR-scr (Fig. 3B). In the cell culture plate, fluorescence signals increased in a miR-193a concentration-dependent manner upon addition of complementary miR-193a (Supplementary information Fig. S5).

3.3. Visualization of miR-193a expression in differentiating neural progenitor cells using FAM-PNA193a-GO molecular beacon

We examined whether FAM-PNA-GO complex could visualize miR-193a expression in differentiated F11 cells as miR-193a was highly expressed in D-F11 cells in qRT-PCR (Fig. 2B). We performed CCK-8 assay to evaluate cytotoxicity of GO in F11 and NE-4C neural stem cells. These cells showed over 90% cell viability upon treatment with GO at concentrations lower than 12.5 μg/mL (Supplementary information Fig. S6). For miRNA sensing, we used GO at 4 μg/mL, which ensures ~100% viability in F11 cells. Addition of GO to FAM-PNA probes completely quenched fluorescence of FAM in opti-MEM medium (Supplementary information Fig. S7). This quenching was not affected in opti-MEM medium while differentiation medium or complete medium increased

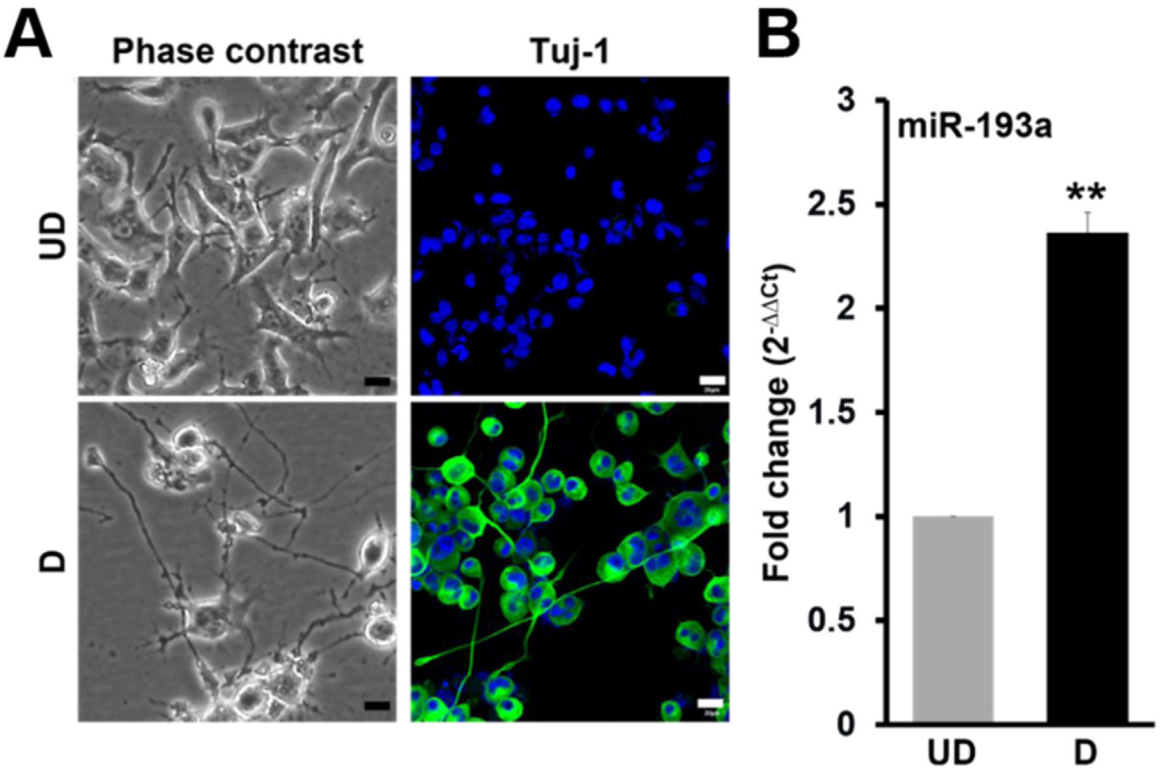

Fig. 2. The enhanced expression of miR-193a in cAMP-induced neuronal differentiation of F11 cells. A) Representative images of phase contrast (left panel) and immunofluorescence staining for Tuj-1 (right panel) in UD- or D-F11 cells. Scale bar, 20 μm. B) Quantitative RT-PCR (qRT-PCR) analysis for the expression of miR-193a in UD- and D-F11 cells. Data is displayed as means ± standard deviation (SD). **P < 0.005. UD: undifferentiated cells, D: differentiated cells.

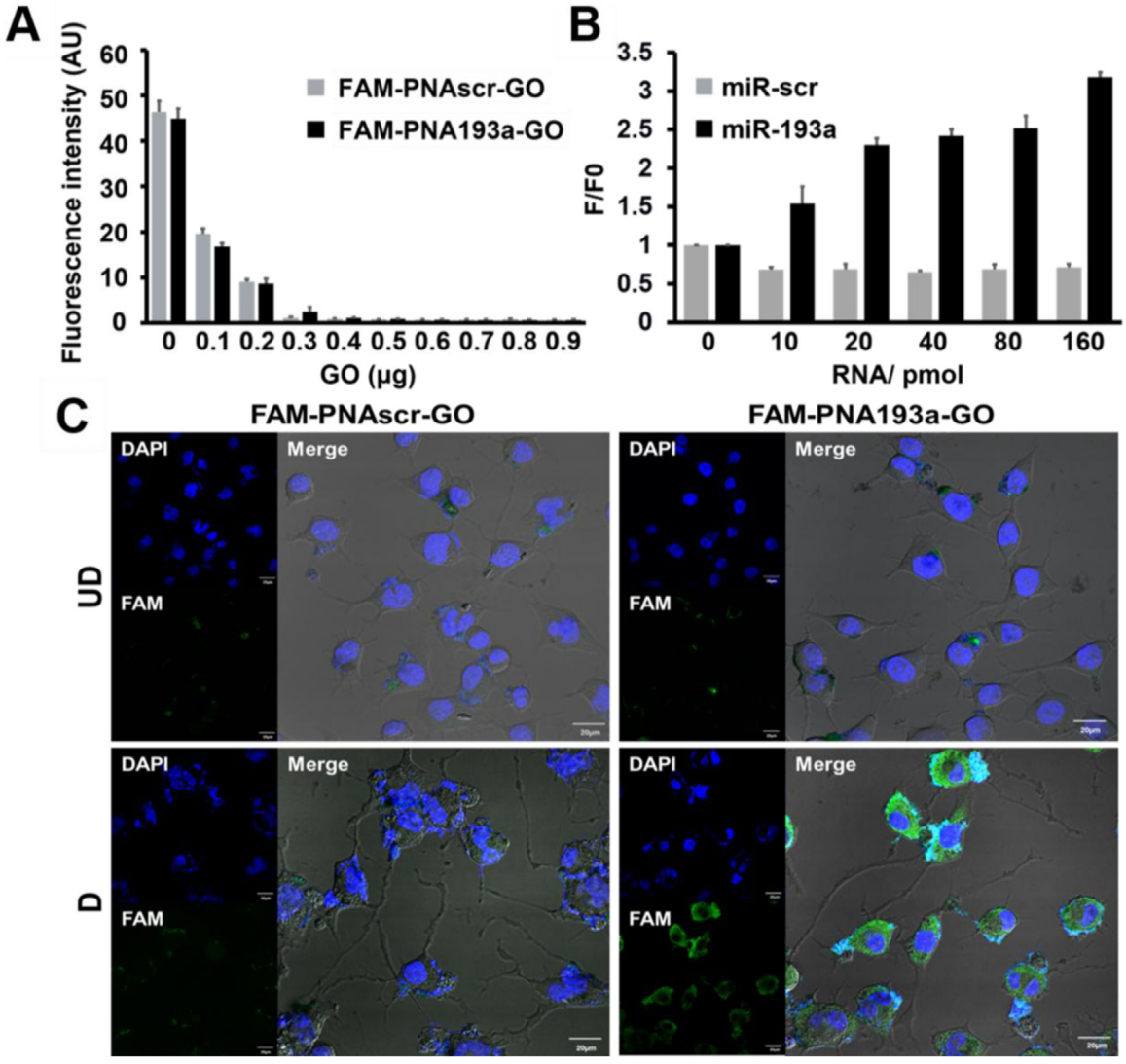

Fig. 3. Specificity test of FAM-PNA193a-GO complex against target miR-193a. A) The fluorescence intensity of FAM-PNA193a and FAM-PNAscr after incubation with GO. Data are displayed as means ± standard deviation (SD). B) Fluorescence recovery of the quenched FAM-PNA probe-GO complex after the addition of miR-scr or miR-193a. Data are displayed as means ± standard deviation (SD). F, fluorescence intensity of FAM-PNA probe-GO complex in the presence of miR-193a oligomer; F0, basal fluorescence intensity of FAM-PNA probe-GO complex without miR-193a treatment. C) Detection of miR-193a 14 h after treatment with FAM-PNA193a-GO or FAM-PNAscr-GO complex in UD- or D-F11 cells. Scale bar, 20 μm. UD: undifferentiated cells, D: differentiated cells.

fluorescence by a small but significant amount (Supplementary information Fig. S8). As miR-193a was up-regulated during neurogenesis in neural progenitor cells, fluorescence signals were observed in the cytoplasm of D-F11 cells treated with FAM-PNA193a-GO while fluorescence was not recovered in D-F11 cells treated with FAM-PNAscr-GO and in UD-F11 cells treated with FAM-PNAscr-GO, or FAM-PNA193a-GO (Fig. 3C).

We validated the selectivity of FAM-PNA193a probe for target miR-193a in differentiated F11 cells after the inhibition of miR-193a expression. miR-193a expression was significantly increased in differentiated F11 cells (Fig. 2B). In a previous study, we confirmed that miR-193a expression and neurogenesis were repressed in differentiating F11 cells in the presence of anti-miR-193a (Oh et al., 2017). Quenched fluorescence signals of FAM-PNA193a-GO were not recovered in differentiating F11 cells after the inhibition of miR-193a expression (Supplementary information Fig. S9). These results suggest that the FAM-PNA193a-GO system provides a highly sensitive and selective method for monitoring changes in endogenous mature miR-193a expression between pre-and post-neuronal differentiation by sensing the increase in miR-193a level during neurogenesis.

3.4. Molecular beacon imaging of miR-193a expression during exosome-mediated neurogenesis on the microfluidic platform

In our previous study (Oh et al., 2017), we confirmed exosomal transport from differentiated to undifferentiated cells through exosome-mediated transport of miR-193a in co-culture, transwell culture and on the microfluidic platform. The exosomes were labeled with RFP fused with CD63 to visualize their migration on the microfluidic chambers from undifferentiated to differentiated F11 cells (Supplementary information Fig. S10). In this microfluidic system, luciferase-laden recipient undifferentiated neural progenitor cells received exosomes by convective flow, and “signal off” of luminescence signified the functional effects of exosome-mediated miR-193a delivery from differentiated cells (Oh et al., 2017).

In the current investigation, we used FAM-PNA193a-GO molecular beacon to monitor the expression of miR-193a by exosome-mediated neurogenesis. We designed a microfluidic platform to elucidate functional outcomes of exosome-mediated miRNA delivery in a recipient chamber with convective flow from the donor chamber that contained differentiated neural progenitor cells (Fig. 4A). Donor F11 cells were

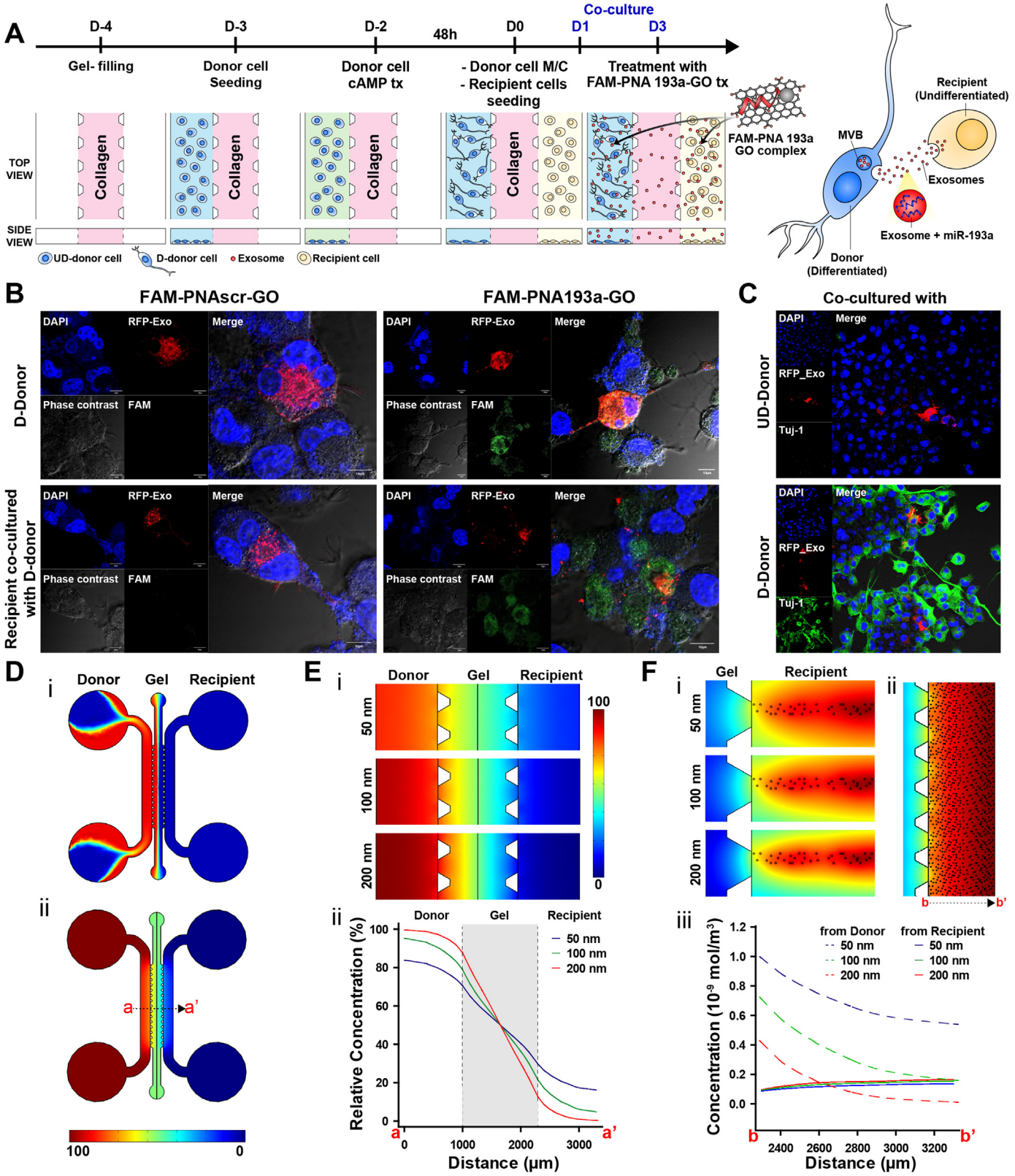

Fig. 4. Neurogenic miR-193a sensing during exosome-mediated neurogenesis in the microfluidic assay. A) Schematic representation of the microfluidic cell culture assay (left panel) and exosome-mediated miR-193a transfer from donor D-F11 cells to recipient UD-F11 cells (right panel). B) Representative fluorescence images showing donor D-F11 cells or recipient F11 cells 14 h after treatment with FAM-PNA193a-GO. Scale bar, 10 μm. C) Immunofluorescence staining for Tuj-1 in recipient F11 cells cultured with RFP-exosome-releasing donor UD- or D-F11 cells. Scale bar, 20 μm. D) Two-step simulation for exosomal transport from donor D-F11 cells in the microfluidic system: i) convective transport by adding culture medium to all reservoirs; ii) diffusive transport after hydrostatic equilibrium. E) The simulation i) images and ii) profiles for relative concentrations of exosomes (50–200 nm) at 24 h. F) The simulation images of i) fractional nD-F11 cells and ii) total nD-F11 cells in recipient channel. iii) The concentration of exosomes transported from donor D-F11 cells and nD-F11 cells at 24 h.

seeded into the left cell culture channel and cultured with differentiation medium containing db-cAMP to induce neurogenesis. After 48 h, once donor cells were considered to have differentiated, recipient F11 cells were seeded into the right channel. Three days after co-culture in both channels, D-donor cells or recipient cells co-cultured with D-donor cells were treated with FAM-PNA193a-GO molecular beacon for 14 h in opti-MEM medium, and then observed using fluorescence confocal microscopy.

Fluorescence from D-donor cells and recipient cells cultured with D-donor cells was recovered from the dark background. This fluorescence represented FAM-PNA193a detachment through the reaction of miR-193a in exosomes of D-donor cells and uptake by recipient cells from exosomes delivered convectively through the gel channel from differentiated cells of donor cell channel (Fig. 4B). Fluorescence of recipient cells was barely visible in recipient cells cultured with undifferentiated donor cells (Supplementary information Fig. S11).

3.5. Heterogeneity of exosome and miR-193a delivery and consequent neural differentiation marker in recipient neural progenitor cells

Exosomes labeled with CD63-RFP released from donor UD- and D-F11 cells moved to and were taken up by recipient F11 cells similarly (Supplementary information Fig. S11, red dots). Recipient UD-F11 cells which took up exosomes recovered fluorescence of PNA193a-GO molecular beacon, as did their neighboring cells. In contrast, some recipient F11 cells did not recover fluorescence despite having taken up exosomes. The agreement of cellular exosome uptake and delivery of miR-193a in these exosomes were easily recognized by observing individual recipient F11 cells. In the individual recipient cells, differences in the amount of miR-193a loaded in donor exosomes (or donor exosomes without miR-193a) would have resulted in variable fluorescence recovery. We also observed some recipient cells with positive fluorescence recovery without having taken up exosomes. Notably, almost all recipient F11 cells showed homogeneous Tuj-1 expression regardless of exosome uptake. In addition to recipient F11 cells with exosome uptake, other recipient cells without CD63-RFP fluorescence showed homogeneous Tuj-1 expression (Fig. 4C). On the microfluidic platform with two channels separated by an intervening gel channel, exosome delivery was observed upon convective media flow from donor to recipient channels in both differentiated and undifferentiated F11 cells. When the donor cells were differentiated F11 cells, exosome uptake in the recipient cells and consequent miR-193a delivery were heterogeneous but Tuj-1 expression was homogeneous. Nevertheless, when donor cells were undifferentiated F11 cells, neither miR-193a expression nor Tuj-1 expression were observed. Similar results were obtained when PNAscr-GO molecular beacon was used.

3.6. Simulation of exosome transport from donor D-F11 cells to recipient nD-F11 cells on the microfluidic platform

To explain the homogeneous Tuj-1 expression levels regardless of fractional exosome uptake in recipient cells, we performed a two-step simulation to investigate exosome transport on the microfluidic system. We designed a two-step simulation process: first, a simulation of the initial convective transport caused by adding medium; second, a simulation of diffusive transport after hydrostatic equilibrium (Fig. 4Di and ii). Exosomes (50–200 nm) secreted from donor D-F11 cells were simulated at 24 h after co-culture (Fig. 4Ei). The results demonstrated that sufficient amounts of exosomes (about 13–30%) delivered to recipient cells by convection and diffusion induced differentiation in some recipient cells (Fig. 4Eii). To elucidate homogenous Tuj-1 expression in recipient cells, we presumed that some differentiated recipient cells released exosomes to induce neurogenesis, which were taken up by adjacent recipient UD-F11 cells. We simulated exosome concentrations from recipient D-F11 cells assumed to be approximately 15% in all recipient cells, which caused cascade exosome delivery to adjacent recipient UD-F11 cells (Supplementary information Fig. S2). The simulation results at 24 h indicated that exosomes released from a small population of recipient D-F11 cells were delivered to adjacent recipient UD-F11 cells (Fig. 4Fi). The simulation results for the concentration profiles of exosomes revealed that exosomes delivered from donor D-F11cells and secreted from newly differentiated (nD) recipient F11 cells were uniformly distributed and sufficiently exposed to all recipient F11 cells (Fig. 4Fii and iii).

4. Discussion

Neurogenic miRNAs play key roles in regulating relevant gene expression for neurogenesis in neural development (Åkerblom and Jakobsson, 2014; Chen et al., 2004; Makeyev et al., 2007). In neuronal cells, activity plays a regulatory role in miRNA turnover, which is generally rapid (Krol et al., 2010). Activity-dependent stimulation of glutamate receptor produced mature miRNA in dendrites and somata in a spatially localized manner (Sambandan et al., 2017). Understanding the roles of dynamic miRNA expression in neuronal cells in physiology and pathology, requires elucidation of the temporal and spatial expression of mature miRNA. In this regard, the development of a highly sensitive sensing platform to detect mature miRNAs will be critical. This developmental endeavor ranges from studies of neuronal development or differentiation-related changes to studies of temporally and spatially localized expression of mature miRNAs participating in various physiologic or pathologic processes. To further understand the cell-autonomous roles of miRNA in neuronal lineage cells, it is necessary to elucidate intercellular neuronal communication with either macromolecules such as peptides or lipid mediators or using exosomes containing packaged nucleic acids, peptides, or other small molecular mediators. How intercellular communication *via* exosomes contributes to the differentiation of neural stem cells is not understood. To understand this cell-non-autonomous phenomenon, a method for visualizing the delivery and action of mediators such as miRNA in individual cells is required. In our previous study (Oh et al., 2017), we used three methods of 2D co-culture, transwell co-culture and microfluidic assay to investigate donor-recipient communications *via* exosomes within clones of neural progenitor cells at different stages of differentiation. We demonstrated that exosome transfer of miR-193a was an intercellular communication mechanism heralding messages concerning neuronal differentiation from preceding differentiated cells to recipient cells. On the microfluidic platform, we divided firstly differentiated cells and undifferentiated cells into separate channels and generated a convective flow of media from donor to recipient cell channels. We confirmed that miR-193a was transferred *via* the exosomes from differentiated donor cells to undifferentiated recipient cells to induce neurite outgrowth and the expression of neural markers in recipient cells. The functional outcome of successful miRNA delivery was verified using recipient cells containing the transgene of miR-193a-complementary target sequences in the 3′UTR of luciferase transgene. Luciferase activity was clearly decreased in recipient undifferentiated cells after receiving exosome-mediated miR-193a on this microfluidic platform (Oh et al., 2017). However, in our previous study, it was necessary for neural progenitors to be selected clonally with transgenes integrated into their chromosomes, and the “signal off” nature of the luciferase reporter necessitated concomitant verification that the cells were not mostly dying or already dead.

To overcome this limitation, the molecular beacon imaging system based on “signal on” methods was developed. Molecular beacon imaging system has been repeatedly reported extensively in the literature (Hwang et al., 2010; Peng et al., 2005; Tan et al., 2004). It has the advantage of visualizing individual cell clusters, allowing elucidation of whether mature miRNAs work in specific spatial or temporal sequences *in vivo* (Hwang et al., 2010) as well as *in vitro* (Ryoo et al., 2013). Conventional miRNA detection methods such as Northern blotting, microarrays and qRT-PCR are labor-intensive, time-consuming and

costly (Ma et al., 2018; Wang et al., 2016). In particular, these methods require the sample to be lysed for isolating intracellular miRNA. One of the most promising tools for miRNA sensing, surface-enhanced Raman scattering (SERS) platform, has many advantages including low background signal, high sensitivity and multiplexing. However, the SERS platform has difficulties detecting miRNAs in living cells, due to miRNA isolation by cell lysis (Jiang et al., 2018). Although intracellular miRNA detection by the SERS platform became possible in recent years (Ye et al., 2017), visualization and real-time monitoring of intracellular miRNA was accomplished by the fluorescence-based molecular beacon system, which provided simpler and more sensitive imaging compared to SERS imaging using Raman microscopy. In the current study, we used miRNA sensing method with PNA-GO probe which was successfully used to detect multiple miRNAs in living cells with high sequence specificity and low background signal (Ryoo et al., 2013). The capacity of GO as a delivery vehicle to the cytoplasm, robust quenching of attached FAM, and easy detachability of single-stranded nucleic acids attached to them by their complementary sequenced miRNAs allows multiplexing (Ryoo et al., 2013) and discovery of differential single-base mismatches of target miRNAs (Lee et al., 2015). GO interacts with target miRNA through π–π stacking interactions including non-covalent Van der Waals forces, which are relatively weaker than ionic bonds or covalent bonds. In the nanographene sensor, the PNA probe, which has a complementary sequence to target miRNA, interacts on the nanographene surface based on π–π interactions. As the hybridization energy between the target miRNA and PNA probe is higher than the π–π interaction energy between the PNA probe and graphene surface, FAM-PNA can be separated from the graphene surface. This displacement is dependent on the sequence of PNA, hence an *in vitro* recovery test (dose-dependent treatment of target RNA sequence in a tube) should be performed. In this regard, PNA was reported to be superior to classical nucleic acids as their delivery with GO vehicle through the cell membrane was easier, and their detachability from GO was guaranteed when the molecular beacon met the relevant miRNAs in the cytoplasm.

In this investigation, we used fluorescent dye FAM-labeled molecular beacon, FAM-PNA-GO as the imaging tool to visualize mature miRNA action *in vitro*. PNA-GO probes were reported to minimize nonspecific fluorescence and also provide sensitive and single-base specific response to target mature miRNAs with low background fluorescence signals with very low cytotoxicity even in living cells (Ryoo et al., 2013). GO exhibits a dose-dependent increase in toxicity (roughly 10–200 μg/mL *in vitro*) and *in vivo* (Li et al., 2014; Zhang et al., 2014). Dose- and time-dependent decrease in cytotoxicity was also observed to be more than 50 μg/mL and 48 h. PNA have also little or no toxicity *in vitro*, and could be administered systematically (Fabani et al., 2010; Sazani et al., 2002). Therefore, we exploited these advantages for molecular beacon imaging of recipient cells on the microfluidic platform. The microfluidic cell culture platform enabled us to observe cell-cell interactions at high resolution in real time while allowing easy modification or control of the sophisticated fluidic system (Shin et al., 2012). We used the same miRNA-sensing microfluidic platform as that in our previous study (Oh et al., 2017) but with “signal-on” molecular beacon of FAM-labeled PNA-GO complex to detect the presence of neurogenic mature miR-193a delivered by exosomes while varying interstitial flow to simulate *in vivo* conditions. This microfluidic platform allowed sequential seeding and precedent induction of neurogenesis in donor cells and observation of recipient cells receiving exosomes and their contents. In these microfluidic channels, both the donor and recipient cells were kept viable by daily medium replacement, in contrast to conventional transwell co-culture studies (Oh et al., 2017; Shin et al., 2012). Furthermore, this microfluidic platform allowed repeated observation of the recipient channel cells using standard confocal microscopes and thus enabled the visualization of molecular beacon “signaling on” within the recipient cells. As miR-193a was expressed during neurogenesis and was transferred *via* exosomes from differentiated cells to undifferentiated cells on the microfluidic platform, we used FAM-PNA193a-GO as the molecular beacon for imaging on the microfluidic platform. On this platform, miR-193a was highly expressed in recipient cells at all 3 days of co-culture, but neurite outgrowth started 2 days after co-culture, and neural markers appeared 3 days after co-culture (Oh et al., 2017). These results suggest that exosomal miR-193a from differentiated donor cells induces neurogenesis of undifferentiated recipient cells initially. This promotes miR-193a action in recipient cells that uptake exosomes, which triggers the sequential process of neurogenesis. However, further studies are required to elucidate whether the recipient cells that have taken up exosomes differentiate alone, whether adjacent cells also differentiate, and whether neurogenic miR193a-induced differentiating neurons begin to differentiate into neurons and recover fluorescence as secondary (or tertiary) endogenous miR-193a expression. In Fig. 4B, CD63-RFP-bound exosomes derived from donor cells were taken up by a certain portion of recipient cells, which showed recovery of FAM fluorescence, indicating the presence of mature miR-193a. Notably, the cells adjacent to the differentiation-labeled cells which received CD63-RFP exosomes also showed recovery of FAM fluorescence. We speculate that the exosomal delivery of neurogenic miR-193a commences differentiation in the recipient cells but also delivers the same or other neurogenic messages to adjacent cells in a cell-non-autonomous way. Neuronal marker expression in the recipient cells in Fig. 4C was more extensive in adjacent cells despite not having received any exosomes from donor cells (absence of CD63-RFP). This implies that there may be cascade delivery between undifferentiated cells in the recipient channel. We did not confirm whether the secondary transfer from CD63-RFP-positive to CD63-RFP-negative recipient cells were also mediated by exosomes, but this may have been the case if the cascade of neurogenesis occurred *via* miR-193a containing exosomes. We propose that FAM-PNA-GO probe can act as molecular beacon imaging tool capable of detecting the presence of miR-193a during neurogenesis in neural progenitor cells in a cell-non-autonomous fashion. Fluorescence of quenched FAM-PNA193a-GO probe was not recovered by miR-scr oligomer (Fig. 3B). Fluorescence recovery of FAM-PNA193a-GO with matching complementary miRNAs was dose dependent. Transmembrane cytoplasmic uptake of molecular beacon made of GO and PNA was homogenous; we observed fluorescence recovery in every cell of cAMP-stimulated differentiated clones (Fig. 3C, lower right picture). Although the background was dark when donor cells were undifferentiated, we could observe CD63-RFP in the recipient cells. When the donor cells were differentiated but the molecular beacon was FAM-PNAscr-GO with scrambled sequences, we observed no fluorescence recovery in the recipient cells regardless of CD63-RFP signals in the cells indicating the presence or absence of exosome delivery (Supplementary information Fig. S11). We propose that this molecular beacon of FAM-PNA193a-GO can be used for visualization of individual cellular responses to exosome-mediated miRNA delivery and transfer in a sensitive and specific way with minimal background in living cells. The heterogeneity of exosome access to the cells despite the assumed ready uptake by recipient cells, and temporally sequential transfer of differentiation message to adjacent cells from cells that first encounter the message may recapitulate conditions *in vivo*. Precedent differentiating cells responding to an internal clock or certain external stimuli may recruit adjacent cells using exosomal delivery of appropriate message to adjacent cells to enact the differentiation process in a sequential manner. This will create a gradient of apparently synchronous differentiation, and the individual cellular responses to the messages received from the “donor” cells may appear heterogeneous. Blotting, qRT-PCR, or assays employing tens or thousands of cells cultured *in vitro* will obscure the nuances of this spatiotemporal information. Individual miRNAs in neurons turn over rapidly in physiologic or pathologic conditions in dendrites of cerebral neurons (Sambandan et al., 2017) and peripheral nerve axons (Krol et al., 2010). This fast turnover was observed for neuron-enriched miRNAs such as miR-9, miR-125b, and miR-146a, which have half-lives of 1–3.5 h (Zhang et al., 2012). The rapid turnover of neuron-specific

miRNAs is dependent on neuronal activity (Krol et al., 2010). Neurons in the hippocampus exhibit activity-dependent maturation of pre-miRNAs in dendrites that respond to stimulus activity (Sambandan et al., 2017). Based on these findings, localized miRNA maturation was proposed to modulate target gene expression with spatial and temporal precision. We propose our molecular beacon imaging using fluorescent dye-PNA (against a specific miRNA)-GO complex as probes has good cellular uptake, but the sequential imaging of cells of interest will reveal the temporal and spatial details of intercellular message transfer during physiologic or pathologic processes.

The important caveats of using our GO quenching-based molecular beacon imaging for characterizing the responses of individual cells at single cell level, are 1) sufficient amount of GO molecular beacon should be administered so that the recovered fluorescence is homogeneous, 2) cells should be located in the recipient chamber of the microfluidic device and should be individually discernible, and 3) dose-response relationships according to the amount of a specific active mature microRNA allows characterization of the quantity (activity) of microRNAs contained in the exosomes. Secondary, tertiary, or further signal transfer between recipient cells warrants future investigation as differentiation markers indicated that all cells eventually participated in the differentiation; a more refined platform will be needed to dissect this cell-cell interaction. Homogeneous Tuj-1 expression of secondary recipient cells provokes speculation regarding the plausible phenomena induced by exosomes and their contents released from recipient cells that are beginning differentiation, and whether they mediate the secondary outcomes or whether new biomolecules mediated this signal transfer resulting in secondary Tuj-1 expression. Although we used preceding differentiating cells and undifferentiated cells of the same clones, the microfluidic platform will allow the use of cells of different germinal origins.

5. Conclusion

In conclusion, we have demonstrated that the exosome-tracing microfluidic platform and miRNA sensing strategy based on fluorescent dye-PNA (against a specific miRNA)-GO complex can be applied to visualize exosomes and to monitor individual cellular expression of mature microRNAs. This system enables precise spatial localization of intercellular exosomes in differentiating F11 cells. The fluorescent-labeled PNA-GO complex was highly sensitive and selective to target miRNA without nonspecific fluorescence signal in differentiating F11 cells. This miRNA sensing platform is applicable for biosensing and bioimaging applications such as miRNA detection for biomarkers in a variety of diseased tissues and monitoring the turnover of specific miRNAs during neural activity and stem cell differentiation.

Acknowledgements

This research was supported by Basic Science Research Program through the National Research Foundation of Korea (NRF) funded by the Ministry of Education (NRF-2017R1A6A3A01007423), and Radiation Technology R&D program through the National Research Foundation of Korea founded by the Ministry of Science and ICT (NRF-2017M2A2A7A02019899), and by the National Research Foundation of Korea (NRF-2017R1A2B3007701) grant funded by the Korea government(MEST), and by a grant of the Korea Health Technology R&D Project through the Korea Health Industry Development Institute (KHIDI), funded by the Ministry of Health & Welfare, Republic of Korea (HI14C3344 and HI14C1277), and National Research Foundation of Korea grant funded by the Korea government (MSIP) (2015M3C7A1028926 and 2017M3C7A1048079).

Competing interest

The authors declare no competing financial interest.

Appendix A. Supporting information

Supplementary data associated with this article can be found in the online version at doi:10.1016/j.bios.2018.11.027.

References

Åkerblom, M., Jakobsson, J., 2014. Neuroscientist 20, 235–242.
Bartel, D.P., 2004. Cell 116, 281–297.
Calin, G.A., Croce, C.M., 2006. Nat. Rev. Cancer 6, 857–866.
Chen, C.Z., Li, L., Lodish, H.F., Bartel, D.P., 2004. Science 303, 83–86.
Delaloy, C., Liu, L., Lee, J.A., Su, H., Shen, F., Yang, G.Y., Young, W.L., Ivey, K.N., Gao, F.B., 2010. Cell. Stem Cell. 6, 323–335.
Deregibus, M.C., Cantaluppi, V., Calogero, R., Lo Iacono, M., Tetta, C., Biancone, L., Bruno, S., Bussolati, B., Camussi, G., 2007. Blood 110, 2440–2448.
Driskell, J.D., Tripp, R.A., 2010. Chem. Commun. 46, 3298–3300.
Duan, D., Zheng, K.X., Shen, Y., Cao, R., Jiang, L., Lu, Z., Yan, X., Li, J., 2011. Nucleic Acids Res. 39.
Eskildsen, T., Taipaleenmaki, H., Stenvang, J., Abdallah, B.M., Ditzel, N., Nossent, A.Y., Bak, M., Kauppinen, S., Kassem, M., 2011. Proc. Natl. Acad. Sci. USA 108 (15), 6139–6144.
Fabani, M.M., Abreu-Goodger, C., Williams, D., Lyons, P.A., Torres, A.G., Smith, K.G.C., Enright, A.J., Gait, M.J., Vigorito, E., 2010. Nucleic Acids Res. 38, 4466–4475.
Fang, S., Lee, H.J., Wark, A.W., Corn, R.M., 2006. J. Am. Chem. Soc. 128, 14044–14046.
Gagan, J., Dey, B.K., Layer, R., Yan, Z., Dutta, A., 2011. J. Biol. Chem. 286, 19431–19438.
Hanvey, J.C., Peffer, N.J., Bisi, J.E., Thomson, S.A., Cadilla, R., Josey, J.A., Ricca, D.J., Hassman, C.F., Bonham, M.A., Au, K.G., Carter, S.G., Bruckenstein, D.A., Boyd, A.L., Noble, S.A., Babiss, L.E., 1992. Science 258 (5087), 1481–1485.
Hartig, J.S., Grüne, I., Najafi-Shoushtari, S.H., Famulok, M., 2004. J. Am. Chem. Soc. 126, 722–723.
He, L., Hannon, G.J., 2004. Nat. Rev. Genet. 5, 522–531.
Hwang, D.W., Lee, D.S., 2012. Nucl. Med. Mol. Imaging 46, 1–9.
Hwang, D.W., Song, I.C., Lee, D.S., Kim, S., 2010. Small 6, 81–88.
Jiang, Y., Sun, D.W., Pu, H., Wei, Q., 2018. Trends Food Sci. Technol. 75, 10–22.
Jing, L., Jya, Y., Lu, J., Han, R., Li, J., Wang, S., Peng, T., Jia, Y., 2011. NeuroReport 22, 206–211.
Karbiener, M., Neuhold, C., Opriessnig, P., Prokesch, A., Bogner-Strauss, J.G., Scheideler, M., 2011. RNA Biol. 8, 850–860.
Kim, H.J., Kim, Y.H., Lee, D.S., Chung, J.-K., Kim, S., 2008. J. Nucl. Med. 49, 1686–1693.
Ko, H.Y., Hwang, D.W., Lee, D.S., Kim, S., 2009. Nat. Protoc. 4, 1663–1669.
Kosaka, N., Iguchi, H., Ochiya, T., 2010. Cancer Sci. 101, 2087–2092.
Krol, J., Busskamp, V., Markiewicz, I., Stadler, M.B., Ribi, S., Richter, J., Duebel, J., Bicker, S., Fehling, H.J., Schübeler, D., Oertner, T.G., Schratt, G., Bibel, M., Roska, B., Filipowicz, W., 2010. Cell 141, 618–631.
Lee, J., Park, G., Min, D.H., 2015. Chem. Commun. 51, 14597–14600.
Lee, J.Y., Kim, S., Hwang, D.W., Jeong, J.M., Chung, J.-K., Lee, M.C., Lee, D.S., 2008. J. Nucl. Med. 49, 285–294.
Lee, Y., Park, J.K., 2017. BioChip J. 11, 308.
Li, T., Shi, L., Wang, E., Dong, S., 2009. Chem. - A Eur. J. 15, 1036–1042.
Li, Y., Wu, Q., Zhao, Y., Bai, Y., Chen, P., Xia, T., Wang, D., 2014. ACS Nano 8, 2100–2110.
Lu, Z., Zhang, L., Deng, Y., Li, S., He, N., 2012. Nanoscale 4, 5840–5842.
Ma, D., Huang, C., Zheng, J., Tang, J., Li, J., Yang, J., Yang, R., 2018. Biosens. Bioelectron. 101, 167–173.
Makeyev, E.V., Zhang, J., Carrasco, M.A., Maniatis, T., 2007. Mol. Cell. 27, 435–448.
Niu, C.S., Yang, Y., Cheng, C.D., 2013. Int. J. Oncol. 42, 1533–1540.
Novina, C.D., Sharp, P.A., 2004. Nature 430, 161–164.
Oh, H.J., Shin, Y., Chung, S., Hwang, D.W., Lee, D.S., 2017. Biomaterials 112, 82–94.
Oh, S.W., Hwang, D.W., Lee, D.S., 2013. Theranostics 3, 1004–1011.
Pegtel, D.M., Cosmopoulos, K., Thorley-Lawson, D.A., van Eijndhoven, M.A.J., Hopmans, E.S., Lindenberg, J.L., de Gruijl, T.D., Wurdinger, T., Middeldorp, J.M., 2010. Proc. Natl. Acad. Sci. USA 107, 6328–6333.
Peng, X.H., Cao, Z.H., Xia, J.T., Carlson, G.W., Lewis, M.M., Wood, W.C., Yang, L., 2005. Cancer Res. 65, 1909–1917.
Pluen, A., Netti, P.A., Jain, R.K., Berk, D.A., 1999. Biophys. J. 77, 542–552.
Pritchard, C.C., Cheng, H.H., Tewari, M., 2012. Nat. Rev. Genet. 13, 358–369.
Pu, F., Huang, Z., Ren, J., Qu, X., 2010. Anal. Chem. 82, 8211–8216.
Ran, X., Wang, Z., Zhang, Z., Pu, F., Ren, J., Qu, X., 2015. Chem. Commun. 7, 5882–5891.
Ratajczak, J., Miekus, K., Kucia, M., Zhang, J., Reca, R., Dvorak, P., Ratajczak, M.Z., 2006. Leukemia 20, 847–856.
Ryoo, S.R., Lee, J., Yeo, J., Na, H.K., Kim, Y.K., Jang, H., Lee, J.H., Han, S.W., Lee, Y., Kim, V.N., Min, D.H., 2013. ACS Nano 7 (7), 5882–5891.
Sambandan, S., Akbalik, G., Kochen, L., Rinne, J., Kahlstatt, J., Glock, C., Tushev, G., Alvarez-Castelao, B., Heckel, A., Schuman, E.M., 2017. Science 355, 634–637.
Sayed, D., Abdellatif, M., 2011. Physiol. Rev. 91, 827–887.
Sazani, P., Gemignani, F., Kang, S.H., Maier, M.A., Manoharan, M., Persmark, M., Bortner, D., Kole, R., 2002. Nat. Biotechnol. 20, 1228–1233.
Shi, H., Sun, H., Yang, H., Liu, S., Jenkins, G., Feng, W., Li, F., Zhao, Q., Liu, B., Huang, W., 2016. Adv. Funct. Mater. 26, 6505.
Shin, Y., Han, S., Jeon, J.S., Yamamoto, K., Zervantonakis, I.K., Sudo, R., Kamm, R.D., Chung, S., 2012. Nat. Protoc. 7, 1247–1259.
Skog, J., Würdinger, T., van Rijn, S., Meijer, D.H., Gainche, L., Curry, W.T., Carter, B.S., Krichevsky, A.M., Breakefield, X.O., 2008. Nat. Cell Biol. 10, 1470–1476.
Sun, W., Julie, Li, Y.-S., Huang, H.-D., Shyy, J.Y.-J., Chien, S., 2010. Annu. Rev. Biomed.

Eng. 12, 1–27.
Tan, W., Wang, K., Drake, T.J., 2004. Curr. Opin. Chem. Biol. 8, 547–553.
Tani, S., Kusakabe, R., Naruse, K., Sakamoto, H., Inoue, K., 2010. Gene 449, 41–49.
Wang, H.N., Crawford, B.M., Fales, A.M., Bowie, M.L., Seewaldt, V.L., Vo-Dinh, T., 2016. J. Phys. Chem. C 120, 21047–21055.
Wang, Y., Zheng, D., Tan, Q., Wang, M.X., Gu, L.Q., 2011. Nat. Nanotechnol. 89, 5124–5130.
Wang, W., Li, L., Ding, M., Luo, G., Liang, Q., 2018. BioChip J. 12, 93.
Ye, S., Li, X., Wang, M., Tang, B., 2017. Anal. Chem. 89, 5124–5130.
Zernecke, A., Bidzhekov, K., Noels, H., Shagdarsuren, E., Gan, L., Denecke, B., Hristov, M., Köppel, T., Jahantigh, M.N., Lutgens, E., Wang, S., Olson, E.N., Schober, A., Weber, C., 2009. Sci. Signal. 2, ra81.
Zhang, Y., Petibone, D., Xu, Y., Mahmood, M., Karmakar, A., Casciano, D., Ali, S., Biris, A.S., 2014. Drug Metab. Rev. 46, 232–246.
Zhang, Z., Qin, Y.W., Brewer, G., Jing, Q., 2012. Rev. RNA 3, 593–600.